AGU PUBLICATIONS

Geophysical Research Letters

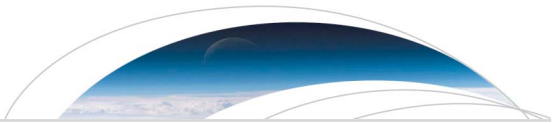

RESEARCH LETTER
10.1002/2017GL072865

Key Points:
- Postseismic velocities over all observed timescales are inversely proportional to time since the earthquake
- Observations are consistent with afterslip or power law creep in a shear zone
- Caution is advised when using near-field sites to infer lower crustal viscosities

Supporting Information:
- Supporting Information S1
- Table S1
- Figure S1
- Figure S2

Correspondence to:
T. Ingleby,
eetfi@leeds.ac.uk

Citation:
Ingleby, T., and T. J. Wright (2017), Omori-like decay of postseismic velocities following continental earthquakes, *Geophys. Res. Lett.*, *44*, 3119–3130, doi:10.1002/2017GL072865.

Received 30 JAN 2017
Accepted 16 MAR 2017
Accepted article online 21 MAR 2017
Published online 14 APR 2017

Omori-like decay of postseismic velocities following continental earthquakes

T. Ingleby[1] **and T. J. Wright**[1]

[1] COMET, School of Earth and Environment, University of Leeds, Leeds, UK

Abstract Various mechanisms have been proposed to explain the transient, enhanced surface deformation rates following earthquakes. Unfortunately, these different mechanisms can produce very similar surface deformation patterns leading to difficulty in distinguishing between them. Here we return to the observations themselves and compile near-field postseismic velocity measurements following moderate to large continental earthquakes. We find that these velocities have a remarkably consistent pattern, with velocity inversely proportional to time since the earthquake. This suggests that postseismic velocities show an Omori-like decay and that postseismic displacements increase logarithmically over time. These observations are inconsistent with simple, linear Maxwell or Burgers body viscoelastic relaxation mechanisms but are consistent with rate-and-state frictional afterslip models and power law shear zone models. The results imply that near-field postseismic surface deformation measurements are primarily the result of fault zone processes and, therefore, that the inference of lower crustal viscosities from near-field postseismic deformation requires care.

1. Introduction

The rheology of the continental lithosphere remains poorly understood, with a number of different disciplines contributing sometimes conflicting observations. Glacial Isostatic Adjustment (GIA) studies in continental cratons suggest that the lithosphere has very high viscosities ($>10^{22}$ Pa s) or behaves elastically [e.g., *Peltier and Drummond*, 2008; *Zhao et al.*, 2012] and generally resolve deep, mantle relaxation with viscosities on the order of $10^{20}-10^{21}$ Pa s. GIA studies examining plate boundary zones find much thinner elastic lithospheric thicknesses and mantle viscosities in the range $10^{18}-10^{19}$ Pa s [*James et al.*, 2000; *Ivins et al.*, 2011]. On shorter timescales, surface deformation following the draining of lakes [e.g., *England et al.*, 2013] and strain concentration associated with interseismic deformation [e.g., *Johnson et al.*, 2007] also suggest relatively high lithospheric viscosities in the range $10^{19}-10^{22}$ Pa s.

Viscosity estimates obtained from early postseismic deformation are typically several orders of magnitude lower than those obtained from other disciplines ($\lesssim 10^{18}$ Pa s) [*Watts et al.*, 2013]. Apparent viscosities are often seen to increase with time since the earthquake leading to inferences of various transient rheologies [e.g., *Pollitz*, 2003; *Ryder et al.*, 2007; *Freed et al.*, 2010]. Whether these inferred viscosities apply to the lower crust, upper mantle or simply the fault zone itself is not always clear [*Bürgmann and Dresen*, 2008; *Wright et al.*, 2013]. Furthermore, the observed surface deformation can also be explained by ongoing fault slip (afterslip) and it is often challenging to distinguish between these competing hypotheses [e.g., *Savage*, 1990; *Perfettini and Avouac*, 2004; *Ryder et al.*, 2007; *Hao et al.*, 2012; *Wright et al.*, 2013]. Despite these common challenges, it has been possible to determine the predominant postseismic deformation mechanism in a selection of cases [e.g., *Jónsson et al.*, 2003; *Freed*, 2007; *Freed et al.*, 2007; *Jónsson*, 2008].

Many studies do not test multiple models against their postseismic data, and so evaluating the relative importance of different deformation mechanisms is challenging. Different authors often reach very different conclusions about the lithosphere using similar observations from the same earthquake [*Wright et al.*, 2013]. For example, postseismic deformation following the 1992 Landers earthquake has been attributed to deep afterslip [*Savage and Svarc*, 1997], poroelastic rebound and deep afterslip [*Fialko*, 2004], afterslip and fault zone contraction [*Massonnet et al.*, 1996], lower crustal relaxation [*Deng et al.*, 1998], and power law mantle flow [*Freed and Bürgmann*, 2004].

Here we compile postseismic observations from 34 moderate to large, continental, intracrustal earthquakes/earthquake sequences. The majority of these observations come from data sources within 25 km

of the coseismic fault. We show that the temporal behavior over timescales from hours to tens of years is remarkably consistent. The results support models in which rate-and-state frictional afterslip and/or viscoelastic relaxation of a power law shear zone are the primary causes of postseismic deformation. We discuss the implications for the rheology of the continental lithosphere.

2. Data Collection

We compiled 151 postseismic velocity data points from 45 publications. These studies cover 34 continental earthquakes/earthquake sequences. The use of the full 3-D deformation field through time provides the most information about postseismic processes and rheology. However, trying to combine this information from multiple earthquakes is challenging. Instead, we combine information about the temporal variation of velocities from multiple earthquakes. In order to collect a consistent data set across different earthquakes and time intervals, we extracted the maximum surface velocities observed in the studied time interval (see Table S1 in the supporting information). If displacements are given at different time intervals for the same earthquake, we use the same observation point (where possible), and this criterion supersedes the criterion of picking the maximum amplitude signal. In other words, if the location of maximal displacement moves with time, we do not follow this and instead extract measurements from the same location through time.

The distance of the maximum deforming surface location from the coseismic fault is a reasonable proxy for the depth range of maximum deformation. Most of the maximum surface velocities come from points in the near-field (Figure 2), which will primarily be affected by near-field, shallow deformation. However, some points are at slightly larger distances; this suggests deeper deformation (e.g., in the lower crust) is dominant.

A variety of measurement techniques were used in the original studies, primarily Global Navigation Satellite Systems (GNSS) (e.g., GPS), interferometric synthetic aperture radar (InSAR), and leveling. GNSS is routinely used to study postseismic deformation; GNSS measurements account for 86 of our 151 data points. In general, horizontal displacements/velocities are reported and we extracted the maximum values, excluding any clear outliers. Interferometric synthetic aperture radar (InSAR) has provided 55 of our 151 data points. InSAR measures the change in distance (range) between the satellite and the ground, equivalent to the projection of the 3-D displacement vector in the satellite line-of-sight (LOS) direction. We chose to extract the maximum postseismic LOS displacement change for each earthquake. This approach may underestimate postseismic deformation if the predominant deformation direction is at a large angle to the satellite look direction. In practice, InSAR is most sensitive to vertical and east-west displacements. Leveling data records changes in height at particular points along transects and is the source of 10 data points in our compilation. The method allows dense spatial coverage along transects but generally has sparse temporal coverage. Nevertheless, it allows us to study postseismic deformation from old earthquakes, for example, from the 1940 Imperial Valley earthquake [*Reilinger*, 1984]. This method is insensitive to horizontal motions, which is problematic for predominantly strike-slip earthquakes.

Isolating a postseismic signal in actively deforming regions of the earth requires the removal of other signals (e.g., interseismic deformation). Most of the studies in our compilation achieve this using data prior to the earthquake or well-established models of other deformation sources. We note those studies where this signal separation is not possible in Table S1 [e.g., *Calais et al.*, 2002; *Vergnolle*, 2003]. The earliest velocity observations included in our compilation are 3.5 h after an earthquake and the latest are 91.5 years after. Postseismic velocities range from over 10,000 mm/yr immediately following an earthquake to less than 1 mm/yr decades later. Using a log-log plot allows us to show the data clearly from all timescales (Figure 1). We connect data points from earthquakes where multiple postseismic deformation rates from different times after the earthquake were available.

In order to examine postseismic velocities at very early times we use data from GPS stations POMM, LAND, and HUNT following the 2004 Parkfield earthquake [*Langbein*, 2006]. We use the 30 min solutions provided by *Langbein* [2006] to examine postseismic velocities very shortly after an earthquake. There is significant scatter in the individual 30 min solutions, but a clear trend is visible in the displacement time series. We perform a piecewise linear fit to the data and extract the postseismic surface velocity over different intervals following the earthquake.

Approximately 100 years after an earthquake, the postseismic signal is only just detectable with current measurement techniques. The latest postseismic velocity estimates we have are those from earthquakes in

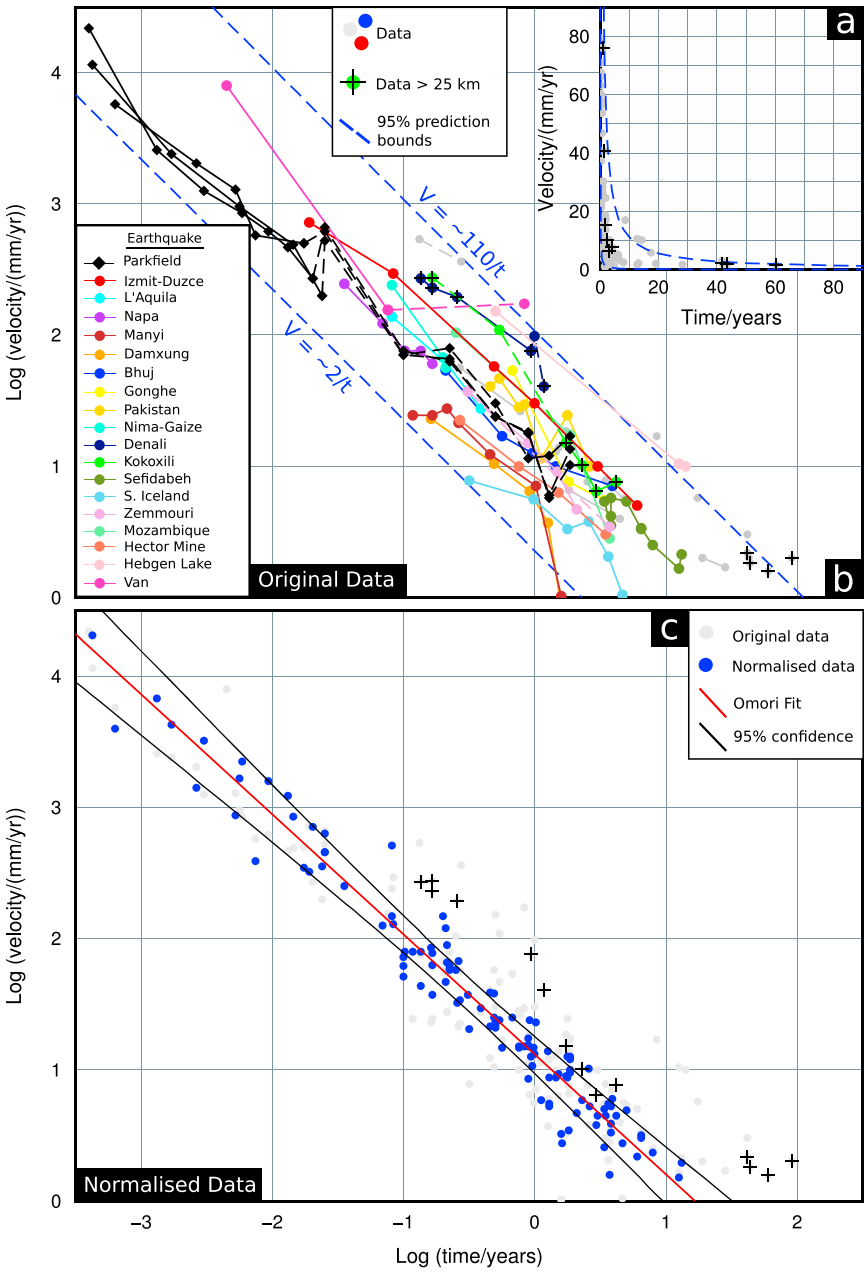

Figure 1. Variation of postseismic surface velocities through time. (a) Zoom showing postseismic velocities over the first 90 years. Rapid, early postseismic velocities are cut off. Grey dots show data, black crosses are data points ⩾ 25 km from the fault. Blue dashes show 95% prediction bounds. (b) Colored lines show time series of postseismic surface velocities from a number of continental earthquakes that display a linear trend in log-log space. Grey data points show data from earthquakes with less than three postseismic observation times. Grey points joined by lines represent earthquakes where only two time series points have been acquired—dashed lines mean those two points came from different studies. Blue dashed lines as in Figure 1a. (c) Normalized results. Light grey circles represent the original data. Blue circles represent the data normalized using intercepts of linear trends through each earthquake time series (see text). Red line shows the best fitting Omori model and black solid lines show the region where 95% of Omori models plot. Data sources: *Barbot et al.* [2008], *Atzori et al.* [2008], *Reddy et al.* [2012], *Calais et al.* [2002], *Hsu et al.* [2002], *Perfettini and Avouac* [2004], *Gourmelen and Amelung* [2005], *Hammond et al.* [2009], *Hetland and Hager* [2003], *Bie et al.* [2013], *Biggs et al.* [2009], *Freed et al.* [2006a], *Pollitz* [2005], *Lammali et al.* [1997], *Pollitz et al.* [2012], *Amoruso et al.* [2005], *Hao et al.* [2012]; *Nishimura and Thatcher* [2003]; *Reilinger* [1986]; *Pollitz and Thatcher* [2010]; *Reilinger* [1984], *Dalla Via* [2005], *Ergintav et al.* [2009], *Diao et al.* [2010], *Ryder et al.* [2011], *Deng et al.* [1998], *D'Agostino et al.* [2012], *Ryder et al.* [2007], *Vergnolle* [2003], *Copley et al.* [2012], *Floyd et al.* [2016], *Ryder et al.* [2010], *Deng et al.* [1999], *Jouanne et al.* [2011], *Barbot et al.* [2009], *Langbein* [2006], *Podgorski et al.* [2007], *Jónsson* [2008], *Copley and Reynolds* [2014], *Copley* [2014], *Riva et al.* [2007], *Dogan et al.* [2014], *Feng et al.* [2014], *Cetin et al.* [2012], and *Mahsas et al.* [2008]

Mongolia, including the *M* 8.4 Bolnay earthquake [*Calais et al.*, 2002; *Vergnolle*, 2003]. These estimates are dependent on models to deconvolve secular, long-lived deformation and transient, postseismic velocities and as such do not represent "raw" observations. Despite this difficulty, the postseismic deformation estimates from these points agree with data from earlier in the postseismic phase.

The data show a remarkably simple trend in log-log space, with a gradient of approximately −1. Postseismic surface velocity (V) is inversely proportional to the time (t) since the earthquake. This trend is evident in individual earthquakes as well as for the whole data set. With these results, we can estimate the range of possible postseismic surface velocities at a given time after an earthquake, assuming a $1/t$ relationship. Ninety-five percent of our postseismic velocities lie between the blue dashed lines in Figure 1, with a factor of approximately 55 separating the lower velocities and higher velocities at any time. This information may be particularly useful for targeting future studies of long-lived postseismic deformation or deploying GNSS stations.

3. Data Analysis

3.1. Normalized Results

There is some scatter in the data which can be attributed to a number of factors. These earthquakes have different magnitudes, depths, and mechanisms, have occurred in different parts of the world, and have been observed using different techniques at different distances from the coseismic fault. However, given the large number of variables which could control postseismic surface velocities, it is surprising how little scatter there is in the data.

A linear regression on each of the individual earthquakes where three or more postseismic velocity measurements were available gave gradients with a mean of −0.96 and a standard deviation of 0.24. Coefficient of determination (R^2) values for these fits were generally high, with most (16 out of 22) higher than 0.9. The slope of the relationship is remarkably similar for all earthquakes, but there is a scale factor that affects the magnitude of postseismic velocities. To remove this effect we normalized each individual earthquake time series. The normalization was based on the linear regression such that the linear fit for each earthquake had a value of 12.16 mm/yr ($\log V = 1.09$) at a time of 1 year ($\log t = 0$); this normalized the results to the mean linear fit to all the data. The normalized results show significant reduction in scatter and have a gradient of -0.92 ± 0.13 (95% confidence interval from Bayesian inversion) close to the average gradient of the individual earthquakes (Figure 1).

3.2. Scaling Factors

We investigate whether these postseismic velocities are dependent on a number of physical properties of the earthquake (moment, depth, and focal mechanism) or are measuring artifacts (distance of the observation from the fault, measuring technique) (Figure 2). Earthquake stress drop is expected to play a significant role in determining the magnitude of any postseismic response. Larger stress drops result in greater stress transfer to neighboring regions of the fault/lithosphere. However, the surface deformation resulting from regions releasing stress depends on how large these regions are (determined by magnitude), and where they are in the lithosphere (determined by depth and focal mechanism). Stress drops are not easily accessible or generally well resolved for all earthquakes in our compilation, and so we do not include this parameter in our analysis. We performed a Bayesian inversion to determine the linear regression coefficients and their errors for magnitude, distance from fault, centroid moment tensor (CMT) depth, and time since the earthquake. Time exerted the strongest control, with magnitude and distance from fault playing secondary roles. We found that larger earthquakes generally produced greater postseismic velocities and that velocities increased with distance from the fault (for distances up to 35 km). CMT depth appeared to play no significant role, but this may be due to large errors in the reported CMT depths.

On a larger scale, there may be scatter due to lateral rheological heterogeneity over the Earth's surface. To test this, we plot each earthquake's power law decay coefficient at the location of the earthquake (see Figures S1a and S1b). We find no clear patterns, although higher decay coefficients are seen in the Tibetan plateau, suggesting that postseismic relaxation may occur more rapidly there. We also examined whether the best fit velocity gradient or intercept varies with time after an earthquake by using the fits to individual earthquakes (see Figures S1c and S1d). There was no clear pattern, with both velocity gradients and intercepts seemingly independent of time since the earthquake.

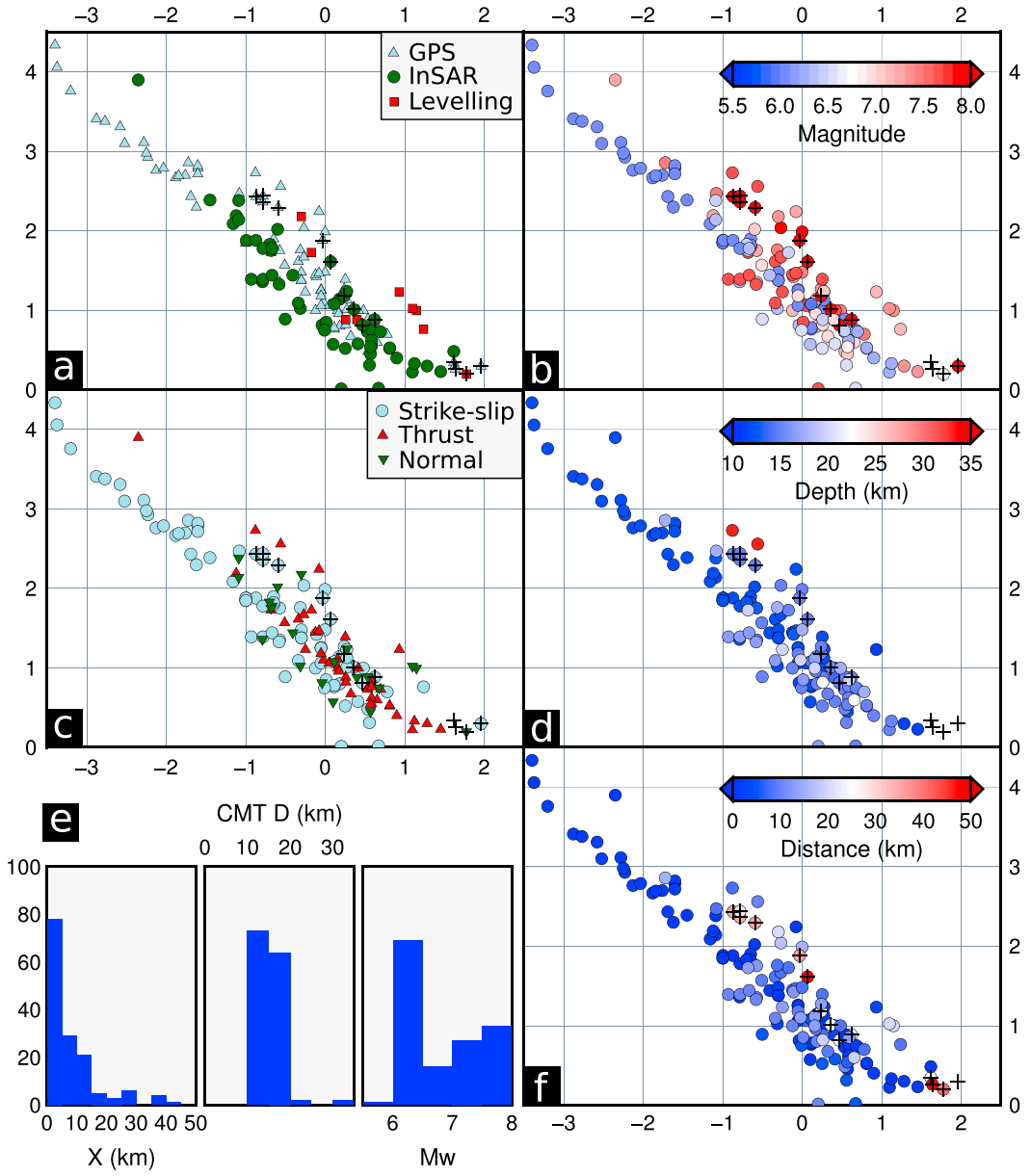

Figure 2. Variation of postseismic deformation results with other possible controls. (a) Variation with observation technique. (b) Variation with moment magnitude of the earthquake. (c) Variation with predominant focal mechanism. (d) Variation with CMT depth. (e) Histograms showing distribution of samples in terms of distance from fault (X), CMT depth and moment magnitude. (f) Variation with perpendicular distance between the measurement point and the fault.

3.3. Consistency With Omori's Law

Our data compilation suggests that postseismic velocities can be fit using a version of Omori's law. *Utsu* [1957] developed the modified Omori's law which describes the number of aftershocks, n, expected at any time, t, after an earthquake:

$$n(t) = \frac{K}{(t+c)^p} \tag{1}$$

Our postseismic velocity compilation can be fit using an equation of the same form, where $n(t)$ is replaced with $V(t)$. We find that p values range between 0.80 and 1.04 (at 95% confidence).

4. Modeling

We use the temporal constraints provided by these observations to test postseismic relaxation models for the crust/upper mantle and fault zones. These models are all based on viscoelastic relaxation or afterslip.

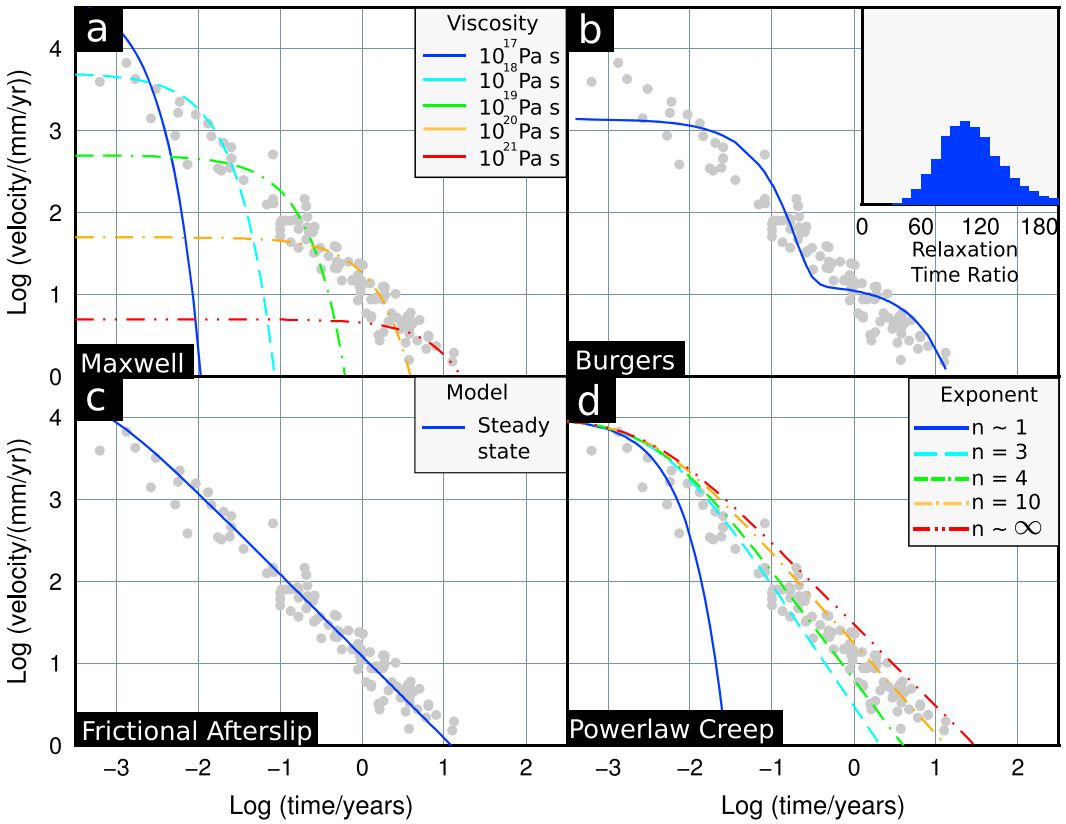

Figure 3. Modeling results. (a) Model runs for Maxwell elements with different viscosities. (b) Maximum likelihood model for a Burgers rheology with two relaxation times. Histogram shows acceptable relaxation time ratios. (c) Maximum likelihood model for a steady state afterslip model. (d) Model runs for power law rheologies with different stress exponents.

We do not consider poroelastic rebound here since this effect is only expected to last a short time following an earthquake [*Jónsson et al.*, 2003; *Fialko*, 2004; *Wright et al.*, 2013].

4.1. Linear Maxwell Models

The simplest rheological model usually invoked to explain postseismic deformation is the linear Maxwell model. A Maxwell material can be conceptualized as an elastic spring and viscous dash pot in series. In an earthquake there is an instantaneous elastic response followed by a decaying response through time as the material relaxes. Postseismic velocity in a Maxwell material will decay exponentially as

$$V(t) = V_0 e^{\frac{-t}{\tau}} \tag{2}$$

where V_0 and τ are constants [e.g., *Montési*, 2004]. The Maxwell relaxation time of the material (τ) is equal to the ratio of viscosity (η) to shear modulus (μ), and the instantaneous velocity (V_0) is inversely proportional to the relaxation time. Although instantaneous postseismic velocities at any time can be matched by this linear Maxwell model, it cannot explain the temporal decay. Low viscosities are required to explain rapid early motions while higher viscosities would be required to explain sustained slow motion (Figure 3).

A slightly more complicated linear rheology is a Burgers body. The Burgers body has a Maxwell material in series with a Kelvin (Voigt) material and shows two relaxation times (τ) [e.g., *Pollitz*, 2003, 2005]. A transient phase of deformation is observed as the Kelvin material relaxes which is superimposed on the longer timescale Maxwell relaxation. Postseismic motion in a Burgers rheology can be described using

$$V(t) = V_0 \left[e^{-\frac{t}{\tau_1}} + K e^{-\frac{t}{\tau_2}} \right] \tag{3}$$

where $\tau_i = \frac{\eta_i}{\mu_i}$, V_0 is a constant initial velocity and K is a scalar [*Malkin and Isayev*, 2012]. The curves produced by these analytical expressions have the same form as those produced using VISCO1D [*Pollitz*, 1992], suggesting

that the use of these expressions is valid. We perform a Bayesian inversion to obtain the maximum likelihood solution for a Burgers body (Figure 3). We find that a 1-D Burgers body model can produce results within the scatter of the data. The acceptable ratios of relaxation times are shown in a histogram in Figure 3. If both relaxing elements have a similar shear modulus, then the ratio in relaxation times can be seen as a ratio in viscosities. We find viscosity ratios of approximately 100 best fit the data. This is larger than the typical ratios found in previous studies [*Ryder et al.*, 2011, and references therein] and is likely due to the need to explain a greater time range of observations simultaneously. Overall, though, the model prediction is inconsistent with the linear log-log trends observed in both the overall data compilation and in individual earthquakes.

Linear Maxwell models and Burgers body models cannot adequately reproduce the temporal evolution observed for postseismic velocities over extended time periods. The addition of more viscoelastic relaxation elements (e.g., a continuum of viscosity values) is able to better reproduce the observed trends [*Hetland and Hager*, 2006]. This viscosity variation may also be in space, for example, with depth [*Riva and Govers*, 2009; *Yamasaki and Houseman*, 2012] or distance from the fault zone [e.g., *Yamasaki et al.*, 2014].

4.2. Afterslip Models

The rate-and-state friction law [*Dieterich*, 1979] has been widely used to explain a number of fault-related phenomena including earthquakes, slow slip events, steady creep, and afterslip. A number of authors have applied the rate-and-state friction law to postseismic afterslip [*Marone*, 1998; *Hearn*, 2002; *Barbot et al.*, 2009]. Rate-and-state friction is often simplified by assuming that the fault is close to the steady state regime. Close to the steady state regime, the state variable is constant in time ($\dot{\theta} = 0$) and there is no loading stress rate. Under these conditions *Marone* [1998] showed that postseismic velocities are

$$V(t) = \frac{V_0}{1 + \frac{t}{\tau}} \tag{4}$$

where τ is a characteristic decay time. In this regime velocity is seen to decay with time following a $1/t$ relationship from an initial value V_0 (Figure 3). This is identical to the modified Omori's law formulation (equation (1)) if $c = \tau$, $K = V_0\tau$ and $p = 1$. The model reproduces the overall temporal decay well.

4.3. Shear Zone Models

Montėsi [2004] investigated postseismic deformation in a power law shear zone and derived a general relaxation law describing postseismic relaxation:

$$V_s(t) = V_0 \left[1 + \left(1 - \frac{1}{n}\right) \frac{t}{\tau}\right]^{\frac{-1}{\left(1-\frac{1}{n}\right)}} \tag{5}$$

where n is the power law exponent. Nonlinear rheologies are those where strain rate is proportional to stress raised to the value of the power law exponent.

This relaxation law allows us to test various shear zone rheologies since the surface velocity is simply expected to be directly proportional to the shear zone velocity. The law simplifies to two end members. When $1/n \to 1$, the general law tends toward the following:

$$V_s(t) = V_0 e^{\frac{-t}{\tau}} \tag{6}$$

This equation defines Newtonian viscous flow in a shear zone and is identical to the linear Maxwell result (equation (2)). This is shown as the blue line in Figure 3d. When $n \gg 1$ and therefore $1/n \to 0$, we obtain the equation for rate-and-state afterslip (equation (4)) [*Montėsi*, 2004]. From postseismic deformation alone, it is impossible to distinguish between postseismic relaxation of a shear zone with high n and frictional afterslip (see red line in Figure 3d). These models are also capable of explaining the overall pattern seen in our postseismic deformation data, provided the power law exponent is greater than the usual range of experimentally determined values.

5. Discussion

5.1. Agreement With Common Postseismic Observations

Our compilation of observations is in agreement with a number of common postseismic observations which we outline below. First, postseismic surface displacement time series are commonly fit using logarithmic

equations [e.g., *Donnellan and Lyzenga*, 1998; *Freed et al.*, 2006a; *Mahsas et al.*, 2008; *Dogan et al.*, 2014]. These equations take the general form

$$x(t) = C \ln\left(1 + \frac{t}{\tau}\right) \tag{7}$$

where C is a constant and τ is a time constant. If this equation is differentiated then we obtain the equation predicted by rate-and-state afterslip and/or relaxation of a high-n shear zone (i.e., $V \propto 1/t$ for high t). Our data also show that postseismic deformation takes an identical functional form to Omori's law describing the decay of aftershocks (equation (1)). Typical p values lie in the range 0.6–2.5 with a median of about 1.1 [*Utsu et al.*, 1995]. Our value for the decay of postseismic surface deformation through time has a p value of about 1 which shows that both postearthquake processes decay at similar rates. Aftershock sequences for continental earthquakes can last for decades to centuries [e.g., *Ryall*, 1977; *Utsu et al.*, 1995; *Ebel et al.*, 2000; *Stein and Liu*, 2009], which is in agreement with the long postseismic deformation timescales included here. Many have noted the similar decay rates of aftershocks and afterslip velocity, leading to the proposition that aftershocks are primarily controlled by frictional afterslip [e.g., *Perfettini and Avouac*, 2004; *Savage et al.*, 2007; *Helmstetter and Shaw*, 2009].

When postseismic relaxation is explained using a viscoelastic material, many authors have noted an apparent increase in crustal/mantle viscosity through time following earthquakes [e.g., *Pollitz*, 2003; *Freed et al.*, 2006a; *Ryder et al.*, 2007]. Our results support this observation and show that this trend continues over a period of 100 years (Figure 3). Maxwell viscoelastic models require an increase in effective viscosity through time in order to match the decreasing postseismic velocities. This changing effective viscosity is sometimes modeled using multiple layers with different viscosity [e.g., *Jónsson*, 2008; *Hetland and Hager*, 2006], a transient rheology like a Burgers body or standard linear solid [e.g., *Pollitz*, 2003, 2005; *Ryder et al.*, 2007, 2011], power law rheologies [e.g., *Freed and Bürgmann*, 2004; *Freed et al.*, 2006b], or a combination of the above. Our compilation shows that any successful model must have a continuously changing viscosity, e.g., power law models with high n or linear models with a large number of relaxation times.

5.2. Temporal Variation and Model Characteristics

We have sampled postseismic deformation over a long time period: from a number of hours after an earthquake up to almost 100 years later. All these data define a linear trend in log-log space with a gradient close to −1. This observation suggests that all continental earthquakes exhibit similar temporal postseismic deformation patterns and allows us to give bounds for expected postseismic velocities at any given time after an earthquake.

Univiscous linear Maxwell materials and Burgers bodies with just two relaxation times cannot reproduce the linear trends seen in our compilation. Viscoelastic models need to be more complex with variations of viscosity in time, space, or both. In sufficiently complex rheologies, the surface displacements can be described by a logarithmic function, which when differentiated will produce a $1/t$ relationship [*Hetland and Hager*, 2006].

Power law creep can reproduce linear trends in log-log space as required by our data. This model is also supported by rock experimental results, but the exponents found in these studies are usually between 2 and 5 [*Carter and Tsenn*, 1987; *Hirth and Kohlstedt*, 2003; *Freed and Bürgmann*, 2004]. Our compilation requires higher power law exponents and suggest that either the experimental results cannot be scaled up to tectonic conditions or more likely, that afterslip is the dominant mechanism recorded by our data.

5.3. Localized Deformation

We find that the temporal variation of our near-field compilation is best explained by afterslip or power law creep at high n. Afterslip is a very localized deformation mechanism, involving continued slip on the fault plane. *Moore and Parsons* [2015] found that a power law rheology contributed to the narrowing of viscous shear zones. They found that narrow shear zones would develop in viscous materials where viscosity varies with depth, with shear stress heating further narrowing the shear zone. Our data are consistent with a localization of postseismic deformation as aseismic afterslip in the upper crust and in deep shear zones in the middle to lower crust.

Fault zone-related processes best explaining our compilation is perhaps not surprising, since our surface velocity measurements are mostly from within a few kilometers of the fault zone (Figure 2). These length scales are certainly small enough to be affected by processes centered on the fault zone [e.g., *Freed*, 2007] and may be dominated by fault zone processes rather than lithospheric relaxation. Furthermore, other strands of

evidence support localized deformation in fault zones. Geodesy reveals that the majority of continental fault zones show significant strain localization between earthquakes [*Wright et al.*, 2013; *Vernant*, 2015]. Geological evidence from exhumed roots of faults shows that motion at depth is likely localized into shear zones up to a few kilometers wide [*Hanmer*, 1988; *Norris and Cooper*, 2003; *Vauchez and Tommasi*, 2003; *Frost et al.*, 2011]. Seismic experiments have also shown deep narrow structures along the North Anatolian Fault in Turkey [*Fichtner et al.*, 2013; *Kahraman et al.*, 2015; *Taylor et al.*, 2016], the San Andreas [*Zhu*, 2000], and dip-slip faults in Tibet [*Zhang et al.*, 2014].

Both afterslip models and power law creep models find support from other observations. Afterslip models can explain the temporal decay in aftershock frequency [*Helmstetter and Shaw*, 2009]. The rate-and-state friction laws which form the basis for the afterslip models used here can also explain a large number of other aspects of the seismic cycle [*Dieterich*, 1994; *Marone*, 1998; *Liu and Rice*, 2005; *Helmstetter and Shaw*, 2009]. At high temperatures and stresses, rocks deform by power law creep in laboratory experiments [*Wilks and Carter*, 1990; *Kohlstedt et al.*, 1995; *Montèsi and Hirth*, 2003; *Bürgmann and Dresen*, 2008]. These conditions may be prevalent in the deeper portions of fault zones.

Fault zone relaxation processes are usually considered to be relatively short-lived, but our data spans decades of the postseismic period. Afterslip has been observed in a few examples decades after earthquakes [*Reilinger*, 1984; *Kaneko et al.*, 2013; *Copley and Reynolds*, 2014; *Copley*, 2014] and often is not tested for on these long timescales. Studies examining postseismic deformation decades after an earthquake should consider the role of continued afterslip, especially for explaining near-fault observations.

While afterslip/power law creep can explain the temporal variation seen in our data, it is unclear whether it can explain the time varying spatial patterns of postseismic deformation. For example, immediately after an earthquake, poroelastic rebound may play a significant role in determining the spatial pattern of postseismic deformation [*Joünsson et al.*, 2003; *Fialko*, 2004] in the near field. Other studies have suggested that broad viscoelastic relaxation of the mantle is required to match far field observations, for example, after the 2002 Denali (Alaska) earthquake [*Freed et al.*, 2006a] or the Landers and Hector Mine earthquakes in California [*Freed et al.*, 2007]. While we argue that the temporal decay of postseismic deformation is a powerful discriminant between competing mechanisms, the spatial patterns of postseismic deformation have been enough to constrain the most important deformation mechanism in a selection of cases [e.g., *Joünsson et al.*, 2003; *Freed et al.*, 2006a; *Freed*, 2007; *Copley et al.*, 2012].

5.4. Implications

Despite these caveats, our findings have some important implications. Our compilation suggests that fault zone processes (afterslip or high n shear zones) generate the largest near-field postseismic signals. These signals may dominate postseismic deformation fields for decades, particularly at near-field sites. As such, caution should be exercised when interpreting lower-crustal viscosities derived from postseismic studies using predominantly near-field data.

Acknowledgments

T.I. is funded by the UK Natural Environment Research Council (NERC) through the Leeds-York NERC Doctoral Training Program (NE/L002574/1). This work was supported by NERC through the Centre for the Observation and Modelling of Earthquakes, Volcanoes and Tectonics (COMET, http://comet.nerc.ac.uk). Figures were made using the Generic Mapping Tools (GMT) [*Wessel and Smith*, 1991]. We thank Andy Hooper and Gregory Houseman for useful discussions. We thank the Editor, Andrew Newman, and Roland Bürgmann and Sylvain Barbot for thoughtful reviews which significantly improved the manuscript. A table with the compilation of postseismic velocities can be found in the supporting information.

References

Amoruso, A., L. Crescentini, E. D'Anastasio, and P. M. D. Martini (2005), Clues of postseismic relaxation for the 1915 Fucino earthquake (central Italy) from modeling of leveling data, *Geophys. Res. Lett.*, *32*, L22307, doi:10.1029/2005GL024139.

Atzori, S., M. Manunta, G. Fornaro, A. Ganas, and S. Salvi (2008), Postseismic displacement of the 1999 Athens earthquake retrieved by the Differential Interferometry by Synthetic Aperture Radar time series, *J. Geophys. Res.*, *113*, B09309, doi:10.1029/2007JB005504.

Barbot, S., Y. Hamiel, and Y. Fialko (2008), Space geodetic investigation of the coseismic and postseismic deformation due to the 2003 M_w 7.2 Altai earthquake: Implications for the local lithospheric rheology, *J. Geophys. Res.*, *113*, B03403, doi:10.1029/2007JB005063.

Barbot, S., Y. Fialko, and Y. Bock (2009), Postseismic deformation due to the M_w 6.0 2004 Parkfield earthquake: Stress-driven creep on a fault with spatially variable rate-and-state friction parameters, *J. Geophys. Res.*, *114*, B07405, doi:10.1029/2008JB005748.

Bie, L., I. Ryder, S. E. J. Nippress, and R. Burgmann (2013), Coseismic and post-seismic activity associated with the 2008 M_w 6.3 Damxung earthquake, Tibet, constrained by InSAR, *Geophys. J. Int.*, *196*, 788–803, doi:10.1093/gji/ggt444.

Biggs, J., R. Burgmann, J. T. Freymueller, Z. Lu, B. Parsons, I. Ryder, G. Schmalzle, and T. Wright (2009), The postseismic response to the 2002 M 7.9 Denali Fault earthquake: Constraints from InSAR 2003–2005, *Geophys. J. Int.*, *176*, 353–367, doi:10.1111/j.1365-246X.2008.03932.x.

Bürgmann, R., and G. Dresen (2008), Rheology of the lower crust and upper mantle: Evidence from rock mechanics, geodesy, and field observations, *Annu. Rev. Earth Planet. Sci.*, *36*, 531–567.

Calais, E., M. Vergnolle, J. Dèverchère, V. San'kov, A. Lukhnev, and S. Amarjargal (2002), Are post-seismic effects of the M = 8.4 Bolnay earthquake (1905 July 23) still influencing GPS velocities in the Mongolia-Baikal area?, *Geophys. J. Int.*, *149*(1), 157–168, doi:10.1046/j.1365-246X.2002.01624.x.

Carter, N. L., and M. C. Tsenn (1987), Flow properties of continental lithosphere, *Tectonophysics*, *136*(1–2), 27–63, doi:10.1016/0040-1951(87)90333-7.

Cetin, E., M. Meghraoui, Z. Cakir, A. M. Akoglu, O. Mimouni, and M. Chebbah (2012), Seven years of postseismic deformation following the 2003 $M_w = 6.8$ Zemmouri earthquake (Algeria) from InSAR time series, *Geophys. Res. Lett.*, *39*, L10307, doi:10.1029/2012GL051344.

Copley, A. (2014), Postseismic afterslip 30 years after the 1978 Tabas-e-Golshan (Iran) earthquake: Observations and implications for the geological evolution of thrust belts, *Geophys. J. Int.*, *197*(2), 665–679, doi:10.1093/gji/ggu023.

Copley, A., and K. Reynolds (2014), Imaging topographic growth by long-lived postseismic afterslip at Sefidabeh, east Iran, *Tectonics*, *33*(3), 330–345, doi:10.1002/2013TC003462.

Copley, A., J. Hollingsworth, and E. Bergman (2012), Constraints on fault and lithosphere rheology from the coseismic slip and postseismic afterslip of the 2006 M_w 7.0 Mozambique earthquake, *J. Geophys. Res.*, *117*, B03404, doi:10.1029/2011JB008580.

D'Agostino, N., D. Cheloni, G. Fornaro, R. Giuliani, and D. Reale (2012), Space-time distribution of afterslip following the 2009 L'Aquila earthquake, *J. Geophys. Res.*, *117*, B02402, doi:10.1029/2011JB008523.

Dalla Via, G. (2005), Lithospheric rheology in southern Italy inferred from postseismic viscoelastic relaxation following the 1980 Irpinia earthquake, *J. Geophys. Res.*, *110*, B06311, doi:10.1029/2004JB003539.

Deng, J., M. Gurnis, H. Kanamori, and E. Hauksson (1998), Viscoelastic flow in the lower crust after the 1992 Landers, California, earthquake, *Science*, *282*(5394), 1689–1692.

Deng, J., K. Hudnut, M. Gurnis, and E. Hauksson (1999), Stress loading from viscous flow in the lower crust and triggering of aftershocks following the 1994 Northridge, California, earthquake, *Geophys. Res. Lett.*, *26*(21), 3209–3212, doi:10.1029/1999GL010496.

Diao, F., X. Xiong, and R. Wang (2010), Mechanisms of transient postseismic deformation following the 2001 M_w 7.8 Kunlun (China) Earthquake, *Pure Appl. Geophys.*, *168*(5), 767–779, doi:10.1007/s00024-010-0154-5.

Dieterich, J. (1994), A constitutive law for rate of earthquake production and its application to earthquake clustering, *J. Geophys. Res.*, *99*, 2601–2618, doi:10.1029/93JB02581.

Dieterich, J. H. (1979), Modeling of rock friction: 1. Experimental results and constitutive equations, *J. Geophys. Res.*, *84*(B5), 2161–2168, doi:10.1029/JB084iB05p02161.

Dogan, U., D. Ö. Demir, Z. Çakir, S. Ergintav, H. Ozener, A. M. Akoglu, S. S. Nalbant, and R. Reilinger (2014), Postseismic deformation following the M_w 7.2, 23 October 2011 Van earthquake (Turkey): Evidence for aseismic fault reactivation, *Geophys. Res. Lett.*, *41*, 2334–2341, doi:10.1002/2014GL059291.

Donnellan, A., and G. A. Lyzenga (1998), GPS observations of fault afterslip and upper crustal deformation following the Northridge earthquake, *J. Geophys. Res.*, *103*(B9), 21285, doi:10.1029/98JB01487.

Ebel, J. E., K.-P. Bonjer, and M. C. Oncescu (2000), Paleoseismicity: Seismicity evidence for past large earthquakes, *Seismol. Res. Lett.*, *71*(2), 283–294, doi:10.1785/gssrl.71.2.283.

England, P. C., R. T. Walker, B. Fu, and M. A. Floyd (2013), A bound on the viscosity of the Tibetan crust from the horizontality of palaeolake shorelines, *Earth Planet. Sci. Lett.*, *375*, 44–56, doi:10.1016/j.epsl.2013.05.001.

Ergintav, S., S. McClusky, E. Hearn, R. Reilinger, R. Cakmak, T. Herring, H. Ozener, O. Lenk, and E. Tari (2009), Seven years of postseismic deformation following the 1999, $M = 7.4$ and $M = 7.2$, Izmit-Düzce, Turkey earthquake sequence, *J. Geophys. Res.*, *114*, B07403, doi:10.1029/2008JB006021.

Feng, W., Z. Li, T. Hoey, Y. Zhang, R. Wang, S. Samsonov, Y. Li, and Z. Xu (2014), Patterns and mechanisms of coseismic and postseismic slips of the 2011 M_w 7.1 Van (Turkey) earthquake revealed by multi-platform synthetic aperture radar interferometry, *Tectonophysics*, *632*, 188–198, doi:10.1016/j.tecto.2014.06.011.

Fialko, Y. (2004), Evidence of fluid-filled upper crust from observations of postseismic deformation due to the 1992 M_w 7.3 Landers earthquake, *J. Geophys. Res.*, *109*, B08401, doi:10.1029/2004JB002985.

Fichtner, A., E. Saygin, T. Taymaz, P. Cupillard, Y. Capdeville, and J. Trampert (2013), The deep structure of the North Anatolian Fault Zone, *Earth Planet. Sci. Lett.*, *373*, 109–117, doi:10.1016/j.epsl.2013.04.027.

Floyd, M. A., et al. (2016), Spatial variations in fault friction related to lithology from rupture and afterslip of the 2014 South Napa, California, earthquake, *Geophys. Res. Lett.*, *43*, 6808–6816, doi:10.1002/2016GL069428.

Freed, A. M. (2007), Afterslip (and only afterslip) following the 2004 Parkfield, California, earthquake, *Geophys. Res. Lett.*, *34*(6), L06312, doi:10.1029/2006GL029155.

Freed, A. M., and R. Bürgmann (2004), Evidence of power-law flow in the Mojave desert mantle, *Nature*, *430*(6999), 548–51, doi:10.1038/nature02784.

Freed, A. M., R. Bürgmann, E. Calais, J. Freymueller, and S. Hreinsdoüttir (2006a), Implications of deformation following the 2002 Denali, Alaska, earthquake for postseismic relaxation processes and lithospheric rheology, *J. Geophys. Res.*, *111*, B01401, doi:10.1029/2005JB003894.

Freed, A. M., R. Bürgmann, E. Calais, and J. Freymueller (2006b), Stress-dependent power-law flow in the upper mantle following the 2002 Denali, Alaska, earthquake, *Earth and Planet. Sci. Lett.*, *252*(3–4), 481–489, doi:10.1016/j.epsl.2006.10.011.

Freed, A. M., R. Bürgmann, and T. Herring (2007), Far-reaching transient motions after Mojave earthquakes require broad mantle flow beneath a strong crust, *Geophys. Res. Lett.*, *34*, L19302, doi:10.1029/2007GL030959.

Freed, A. M., T. Herring, and R. Bürgmann (2010), Steady-state laboratory flow laws alone fail to explain postseismic observations, *Earth Planet. Sci. Lett.*, *300*(1–2), 1–10, doi:10.1016/j.epsl.2010.10.005.

Frost, E., J. Dolan, L. Ratschbacher, B. Hacker, and G. Seward (2011), Direct observation of fault zone structure at the brittle-ductile transition along the Salzach-Ennstal-Mariazell-Puchberg fault system, Austrian Alps, *J. Geophys. Res.*, *116*, B02411, doi:10.1029/2010JB007719.

Gourmelen, N., and F. Amelung (2005), Postseismic mantle relaxation in the Central Nevada seismic belt, *Science*, *310*, 1473–1476, doi:10.1126/science.1119798.

Hammond, W. C., C. Kreemer, and G. Blewitt (2009), Geodetic constraints on contemporary deformation in the northern Walker Lane: 3. Central Nevada seismic belt postseismic relaxation, *Geol. Soc. Am. Spec. Pap.*, *447*, 33–54, doi:10.1130/2009.2447(03).

Hanmer, S. (1988), Great Slave Lake Shear Zone, Canadian Shield: Reconstructed vertical profile of a crustal-scale fault zone, *Tectonophysics*, *149*(3–4), 245–264, doi:10.1016/0040-1951(88)90176-X.

Hao, M., Z.-K. Shen, Q. Wang, and D. Cui (2012), Postseismic deformation mechanisms of the 1990 M_w 6.4 Gonghe, China earthquake constrained using leveling measurements, *Tectonophysics*, *532–535*, 205–214, doi:10.1016/j.tecto.2012.02.005.

Hearn, E. H. (2002), Dynamics of Izmit earthquake postseismic deformation and loading of the Duzce earthquake hypocenter, *Bull. Seismol. Soc. Am.*, *92*(1), 172–193, doi:10.1785/0120000832.

Helmstetter, A., and B. E. Shaw (2009), Afterslip and aftershocks in the rate-and-state friction law, *J. Geophys. Res.*, *114*, B01308, doi:10.1029/2007JB005077.

Hetland, E. A., and B. H. Hager (2003), Postseismic relaxation across the Central Nevada seismic belt, *J. Geophys. Res.*, *108*(B8), 2394, doi:10.1029/2002JB002257.

Hetland, E. A., and B. H. Hager (2006), The effects of rheological layering on post-seismic deformation, *Geophys. J. Int.*, *166*(1), 277–292, doi:10.1111/j.1365-246X.2006.02974.x.

Hirth, G., and D. Kohlstedt (2003), Rheology of the upper mantle and the mantle wedge: A view from the experimentalists, in *Inside the Subduction Factory*, pp. 83–105, AGU, Washington, D. C., doi:10.1029/138GM06.

Hsu, Y.-J., N. Bechor, P. Segall, S.-B. Yu, L.-C. Kuo, and K.-F. Ma (2002), Rapid afterslip following the 1999 Chi-Chi, Taiwan earthquake, *Geophys. Res. Lett.*, *29*(16), 1–4, doi:10.1029/2002GL014967.

Ivins, E. R., M. M. Watkins, D.-N. Yuan, R. Dietrich, G. Casassa, and A. Ruülke (2011), On-land ice loss and glacial isostatic adjustment at the Drake Passage: 2003–2009, *J. Geophys. Res.*, *116*, B02403, doi:10.1029/2010JB007607.

James, T. S., J. J. Clague, K. Wang, and I. Hutchinson (2000), Postglacial rebound at the northern Cascadia subduction zone, *Quat. Sci. Rev.*, *19*(14–15), 1527–1541, doi:10.1016/S0277-3791(00)00076-7.

Johnson, K. M., G. E. Hilley, and R. Bürgmann (2007), Influence of lithosphere viscosity structure on estimates of fault slip rate in the Mojave region of the San Andreas fault system, *J. Geophys. Res.*, *112*, B07408, doi:10.1029/2006JB004842.

Joünsson, S. (2008), Importance of post-seismic viscous relaxation in southern Iceland, *Nat. Geosci.*, *1*(2), 136–139, doi:10.1038/ngeo105.

Joünsson, S., P. Segall, R. Pedersen, and G. Bjoürnsson (2003), Post-earthquake ground movements correlated to pore-pressure transients, *Nature*, *424*(6945), 179–183, doi:10.1038/nature01776.

Jouanne, F., A. Awan, A. Madji, A. Pėcher, M. Latif, A. Kausar, J. L. Mugnier, I. Khan, and N. A. Khan (2011), Postseismic deformation in Pakistan after the 8 October 2005 earthquake: Evidence of afterslip along a flat north of the Balakot-Bagh thrust, *J. Geophys. Res.*, *116*, B07401, doi:10.1029/2010JB007903.

Kahraman, M., D. G. Cornwell, D. A. Thompson, S. Rost, G. A. Houseman, N. Tuürkelli, U. Teoman, S. Altuncu Poyraz, M. Utkucu, and L. Guülen (2015), Crustal-scale shear zones and heterogeneous structure beneath the North Anatolian fault zone, Turkey, revealed by a high-density seismometer array, *Earth Planet. Sci. Lett.*, *430*, 129–139, doi:10.1016/j.epsl.2015.08.014.

Kaneko, Y., Y. Fialko, D. T. Sandwell, X. Tong, and M. Furuya (2013), Interseismic deformation and creep along the central section of the North Anatolian Fault (Turkey): InSAR observations and implications for rate-and-state friction properties, *J. Geophys. Res. Solid Earth*, *118*, 316–331, doi:10.1029/2012JB009661.

Kohlstedt, D. L., B. Evans, and S. J. Mackwell (1995), Strength of the lithosphere: Constraints imposed by laboratory experiments, *J. Geophys. Res.*, *100*(B9), 17,587–17,602, doi:10.1029/95JB01460.

Lammali, K., M. Bezzeghoud, F. Oussadou, D. Dimitrov, and H. Benhallou (1997), Postseismic deformation at El Asnam (Algeria) in the seismotectonic context of northwestern Algeria, *Geophys. J. Int.*, *129*(3), 597–612, doi:10.1111/j.1365-246X.1997.tb04496.x.

Langbein, J. (2006), Coseismic and initial postseismic deformation from the 2004 Parkfield, California, earthquake, observed by Global Positioning System, electronic distance meter, creepmeters, and borehole strainmeters, *Bull. Seismol. Soc. Am.*, *96*, S304–S320, doi:10.1785/0120050823.

Liu, Y., and J. R. Rice (2005), Aseismic slip transients emerge spontaneously in three-dimensional rate and state modeling of subduction earthquake sequences, *J. Geophys. Res.*, *110*, B08307, doi:10.1029/2004JB003424.

Mahsas, A., K. Lammali, K. Yelles, E. Calais, A. M. Freed, and P. Briole (2008), Shallow afterslip following the 2003 May 21, M_w = 6.9 Boumerdes earthquake, Algeria, *Geophys. J. Int.*, *172*(1), 155–166, doi:10.1111/j.1365-246X.2007.03594.x.

Malkin, A. I., and A. I. Isayev (2012), *Rheology: Concepts, Methods, and Applications*, 474 pp., ChemTec Publ., Toronto.

Marone, C. (1998), Laboratory-derived friction laws and their application to seismic faulting, *Annu. Rev. Earth Planet. Sci.*, *26*, 643–696.

Massonnet, D., W. Thatcher, and H. Vadon (1996), Detection of postseismic fault-zone collapse following the Landers earthquake, *Nature*, *382*(6592), 612–616, doi:10.1038/382612a0.

Montėsi, L. G., and G. Hirth (2003), Grain size evolution and the rheology of ductile shear zones: From laboratory experiments to postseismic creep, *Earth Planet. Sci. Lett.*, *211*(1–2), 97–110, doi:10.1016/S0012-821X(03)00196-1.

Montėsi, L. G. J. (2004), Controls of shear zone rheology and tectonic loading on postseismic creep, *J. Geophys. Res.*, *109*, B10404, doi:10.1029/2003JB002925.

Moore, J. D. P., and B. Parsons (2015), Scaling of viscous shear zones with depth-dependent viscosity and power-law stress-strain-rate dependence, *Geophys. J. Int.*, *202*(1), 242–260, doi:10.1093/gji/ggv143.

Nishimura, T., and W. Thatcher (2003), Rheology of the lithosphere inferred from postseismic uplift following the 1959 Hebgen Lake earthquake, *J. Geophys. Res.*, *108*, 2389, doi:10.1029/2002JB002191.

Norris, R. J., and A. F. Cooper (2003), Very high strains recorded in mylonites along the Alpine Fault, New Zealand: Implications for the deep structure of plate boundary faults, *J. Struct. Geol.*, *25*(12), 2141–2157, doi:10.1016/S0191-8141(03)00045-2.

Peltier, W. R., and R. Drummond (2008), Rheological stratification of the lithosphere: A direct inference based upon the geodetically observed pattern of the glacial isostatic adjustment of the North American continent, *Geophys. Res. Lett.*, *35*(16), L16314, doi:10.1029/2008GL034586.

Perfettini, H., and J.-P. Avouac (2004), Postseismic relaxation driven by brittle creep: A possible mechanism to reconcile geodetic measurements and the decay rate of aftershocks, application to the Chi-Chi earthquake, Taiwan, *J. Geophys. Res.*, *109*, B02304, doi:10.1029/2003JB002488.

Podgorski, J., E. H. Hearn, S. McClusky, R. Reilinger, T. Taymaz, O. Tan, M. Prilepin, T. Guseva, and M. Nadariya (2007), Postseismic deformation following the 1991 Racha, Georgia, earthquake, *Geophys. Res. Lett.*, *34*, L04310, doi:10.1029/2006GL028477.

Pollitz, F. F. (1992), Postseismic relaxation theory on the spherical Earth, *Bull. Seismol. Soc. Am.*, *82*(1), 422–453.

Pollitz, F. F. (2003), Transient rheology of the uppermost mantle beneath the Mojave Desert, California, *Earth Planet. Sci. Lett.*, *215*(1–2), 89–104, doi:10.1016/S0012-821X(03)00432-1.

Pollitz, F. F. (2005), Transient rheology of the upper mantle beneath central Alaska inferred from the crustal velocity field following the 2002 Denali earthquake, *J. Geophys. Res.*, *110*, B08407, doi:10.1029/2005JB003672.

Pollitz, F. F., and W. Thatcher (2010), On the resolution of shallow mantle viscosity structure using postearthquake relaxation data: Application to the 1999 Hector Mine, California, earthquake, *J. Geophys. Res.*, *115*, B10412, doi:10.1029/2010JB007405.

Pollitz, F. F., R. Bürgmann, and W. Thatcher (2012), Illumination of rheological mantle heterogeneity by the *M*7.2 2010 El Mayor-Cucapah earthquake, *Geochem. Geophys. Geosyst.*, *13*(6), Q06002, doi:10.1029/2012GC004139.

Reddy, C. D., P. S. Sunil, R. Bürgmann, D. V. Chandrasekhar, and T. Kato (2012), Postseismic relaxation due to Bhuj earthquake on January 26, 2001: Possible mechanisms and processes, *Nat. Hazard.*, *65*(2), 1119–1134, doi:10.1007/s11069-012-0184-7.

Reilinger, R. (1984), Coseismic and postseismic vertical movements associated with the 1940 *M* 7.1 Imperial Valley, California, earthquake, *J. Geophys. Res.*, *89*(B6), 4531, doi:10.1029/JB089iB06p04531.

Reilinger, R. (1986), Evidence for postseismic viscoelastic relaxation following the 1959 *M* = 7.5 Hebgen Lake, Montana, Earthquake, *J. Geophys. Res.*, *91*(B9), 9488, doi:10.1029/JB091iB09p09488.

Riva, R. E. M., and R. Govers (2009), Relating viscosities from postseismic relaxation to a realistic viscosity structure for the lithosphere, *Geophys. J. Int.*, *176*(2), 614–624, doi:10.1111/j.1365-246X.2008.04004.x.

Riva, R. E. M., A. Borghi, A. Aoudia, R. Barzaghi, R. Sabadini, and G. F. Panza (2007), Viscoelastic relaxation and long-lasting after-slip following the 1997 Umbria-Marche (Central Italy) earthquakes, *Geophys. J. Int.*, *169*(2), 534–546, doi:10.1111/j.1365-246X.2007.03315.x.

Ryall, A. (1977), Earthquake hazard in the Nevada region, *Bull. Seismol. Soc. Am.*, *67*(2), 517–532.

Ryder, I., B. Parsons, T. J. Wright, and G. J. Funning (2007), Post-seismic motion following the 1997 Manyi (Tibet) earthquake: InSAR observations and modelling, *Geophys. J. Int.*, *169*(3), 1009–1027, doi:10.1111/j.1365-246X.2006.03312.x.

Ryder, I., R. Bürgmann, and J. Sun (2010), Tandem afterslip on connected fault planes following the 2008 Nima-Gaize (Tibet) earthquake, *J. Geophys. Res.*, *115*, B03404, doi:10.1029/2009JB006423.

Ryder, I., R. Bürgmann, and F. Pollitz (2011), Lower crustal relaxation beneath the Tibetan Plateau and Qaidam Basin following the 2001 Kokoxili earthquake, *Geophys. J. Int.*, *187*(2), 613–630, doi:10.1111/j.1365-246X.2011.05179.x.

Savage, J. C. (1990), Equivalent strike-slip earthquake cycles in half-space and lithosphere-asthenosphere earth models, *J. Geophys. Res.*, *95*(B4), 4873, doi:10.1029/JB095iB04p04873.

Savage, J. C., and J. L. Svarc (1997), Postseismic deformation associated with the 1992 M_w = 7.3 Landers earthquake, southern California, *J. Geophys. Res.*, *102*(B4), 7565–7577, doi:10.1029/97JB00210.

Savage, J. C., J. L. Svarc, and S.-B. Yu (2007), Postseismic relaxation and aftershocks, *J. Geophys. Res.*, *112*, B06406, doi:10.1029/2006JB004584.

Stein, S., and M. Liu (2009), Long aftershock sequences within continents and implications for earthquake hazard assessment, *Nature*, *462*(7269), 87–89, doi:10.1038/nature08502.

Taylor, G., S. Rost, and G. Houseman (2016), Crustal imaging across the North Anatolian fault zone from the auto-correlation of ambient seismic noise, *Geophys. Res. Lett.*, *43*(6), 2502–2509.

Utsu, T. (1957), Magnitude of earthquakes and occurrence of their aftershocks, *Zisin J. Seismol. Soc. Jpn. Ser. 2*, *10*(1), 35–45.

Utsu, T., Y. Ogata, and R. S. Matsu'ura (1995), The centenary of the Omori formula for a decay law of aftershock activity, *J. Phys. Earth*, *43*(1), 1–33, doi:10.4294/jpe1952.43.1.

Vauchez, A., and A. Tommasi (2003), Wrench faults down to the asthenosphere: geological and geophysical evidence and thermomechanical effects, *Geol. Soc. London Spec. Publ.*, *210*(1), 15–34, doi:10.1144/GSL.SP.2003.210.01.02.

Vergnolle, M. (2003), Constraints on the viscosity of the continental crust and mantle from GPS measurements and postseismic deformation models in western Mongolia, *J. Geophys. Res.*, *108*(B10), 2502, doi:10.1029/2002JB002374.

Vernant, P. (2015), What can we learn from 20 years of interseismic GPS measurements across strike-slip faults?, *Tectonophysics*, *644–645*, 22–39, doi:10.1016/j.tecto.2015.01.013.

Watts, A., S. Zhong, and J. Hunter (2013), The behavior of the lithosphere on seismic to geologic timescales, *Annu. Rev. Earth Planet. Sci.*, *41*(1), 443–468, doi:10.1146/annurev-earth-042711-105457.

Wessel, P., and W. H. F. Smith (1991), Free software helps map and display data, *Eos, Trans. AGU*, *72*(41), 441–441, doi:10.1029/90EO00319.

Wilks, K. R., and N. L. Carter (1990), Rheology of some continental lower crustal rocks, *Tectonophysics*, *182*(1–2), 57–77, doi:10.1016/0040-1951(90)90342-6.

Wright, T. J., J. R. Elliott, H. Wang, and I. Ryder (2013), Earthquake cycle deformation and the Moho: Implications for the rheology of continental lithosphere, *Tectonophysics*, *609*, 504–523.

Yamasaki, T., and G. A. Houseman (2012), The crustal viscosity gradient measured from post-seismic deformation: A case study of the 1997 Manyi (Tibet) earthquake, *Earth Planet. Sci. Lett.*, *351–352*, 105–114, doi:10.1016/j.epsl.2012.07.030.

Yamasaki, T., T. J. Wright, and G. A. Houseman (2014), Weak ductile shear zone beneath a major strike-slip fault: Inferences from earthquake cycle model constrained by geodetic observations of the western North Anatolian fault zone, *J. Geophys. Res. Solid Earth*, *119*(4), 3678–3699, doi:10.1002/2013JB010347.

Zhang, Z., Y. Wang, G. A. Houseman, T. Xu, Z. Wu, X. Yuan, Y. Chen, X. Tian, Z. Bai, and J. Teng (2014), The Moho beneath western Tibet: Shear zones and eclogitization in the lower crust, *Earth Planet. Sci. Lett.*, *408*, 370–377, doi:10.1016/j.epsl.2014.10.022.

Zhao, S., K. Lambeck, and M. Lidberg (2012), Lithosphere thickness and mantle viscosity inverted from GPS-derived deformation rates in Fennoscandia, *Geophys. J. Int.*, *190*(1), 278–292, doi:10.1111/j.1365-246X.2012.05454.x.

Zhu, L. (2000), Crustal structure across the San Andreas Fault, Southern California from teleseismic converted waves, *Earth Planet. Sci. Lett.*, *179*(1), 183–190, doi:10.1016/S0012-821X(00)00101-1.